

MINERALOGICAL CHARACTERISTIC OF MORTARS FROM THE TEMPLE OF HATSHEPSUT AT DEIR EL-BAHARI: PRELIMINARY REPORT

Teresa Dziedzic,¹ Wojciech Bartz,² Maria Gąsior³

^{1,3} Wrocław University of Technology, ² University of Wrocław

Abstract: The article presents the results of physico-chemical analyses of a few masonry mortar and whitewash samples taken in the mid-1990s from the Temple of Hatshepsut in Deir el-Bahari. The mineralogical characteristic of the samples contributes to the body of knowledge on the composition of these masonry mortars and their structure, while at the same time encouraging further research on a greater number of samples.

Keywords: mineralogy, physico-chemical analyses, masonry mortar, Deir el-Bahari, Temple of Hatshepsut

Interdisciplinary research on two complexes, that of the Royal Mortuary Cult and the Sun Cult, both constituent parts of the Temple of Hatshepsut in Deir el-Bahari, has been carried out for the past few dozen years. Studies, supported by laboratory analyses, have covered egyptological, archaeological, architectural and conservation issues, bringing significant new information on the structure. Physico-chemical analyses answer questions put by researchers, but the results sometimes raise new ones. The results presented in this article refer to seven samples taken with permission of the Egyptian antiquities authorities in the

mid-1990s, stored in the mission archives and recently subjected to analysis. Six samples were taken of building mortars and one of whitewash. The objective was to identify in detail the mineralogical composition and in consequence to determine whether the structure of the building mortars used in the temple was homogeneous and whether they can say anything about the different building stages of the temple.

MASONRY MORTARS IN ANCIENT EGYPT

Not much has been written on the topic of masonry mortars and whitewash used in

ancient Egypt. The basic publications are: *Ancient Egyptian materials and industries* (Lucas and Harris 1962: 74–76), *Ancient Egyptian construction and architecture* (Clarke and Engelbach 1990: 78–83), *Building in Egypt: Pharaonic stone masonry* (Arnold 1991: 291–293) and *The encyclopedia of ancient Egyptian architecture* (Arnold et al. 2003: 101, 155). Significant information on the use of gypsum binder is included in *Ancient Egyptian materials and technology* (Nicholson and Shaw 2000: 21, 22), a fact already pointed out by the authors of *Cywilizacja miedzi i kamienia* (Lipińska and Koziński 1997: 409). The fullest and most exhaustive information appears in the publications of A. Lucas, S. Clarke and R. Engelbach, as well as D. Arnold, but Lucas alone refers to chemical analyses carried out on many Egyptian materials, not only of the building kind. D. Arnold emphasized the need to continue with further research on mortars used in ancient Egypt.

Egyptian building technique called for mortar to be used as filling in the space between blocks, but without bonding importance for the heavy stone elements owing to its low parameters of mechanical resistance (Clarke and Engelbach 1990: 78). The mortar was composed of unslaked lime, sand and frequently also crushed limestone (Arnold 1991: 291). Gypsum mortar set, but the process was delayed permitting blocks of large format to be mounted and stabilized (Clarke and Engelbach 1990: 80). Gypsum was used also as a binder in render, applied directly to the stone walls of the temple, where their purpose often was to fill in unevenness

and cracks in the surface (Arnold 1991: 292). It was typical render used in ancient Egypt, from the Third Dynasty onwards. There is no evidence for a lime binder being used before the Ptolemaic period (Lucas 1948: 79).¹

The modern word “gypsum” derives from the Akkadian *gassu*, but an Egyptian word, which was lost and is no longer known to researchers, must have existed in the meantime (Arnold 1991: 293). Being a natural material, gypsum is of a uniform color, possibly white, grey, sometimes pink or pale brown. Gray gypsum render/plaster often took the color from microscopic bits of charcoal used to fire the furnaces for calcination of gypsum stone.

Gypsum beds are found in many regions of Egypt, among others as gypsum stone occurring in beds west of Alexandria, between Ismailia and Suez, in Fayum and on the Red Sea coast, as well as broken up concentrations of weakly compacted crystals underground in desert limestone. Gypsum is never pure in nature, containing changing proportions of calcium sulphate, quartz sand and other substances. Lucas examined the chemical composition of many gypsum samples and observed that the gypsum used in Saqqara and Giza contained 97.3%–99.5% pure gypsum and came from Fayum Oasis. He also found that gypsum mortars and plasters were commonly used, because the production of unslaked lime (CaO) from limestone required the stone to be heated to 900°C. Gypsum dehydration temperature ranges from 100°C to 200°C, the process taking place usually at about 130°C (Lucas 1948: 79–80).

¹ According to S. Clarke (Clarke and Engelbach 1990: 79), unslaked lime was not used before the Roman period.

THE TEMPLE OF HATSHEPSUT IN DEIR EL-BAHARI

Queen Hatshepsut (Maatkara) had the title of King of the North and South, but it was seldom used for women in the history of ancient Egypt. Hatshepsut was a pharaoh of the Eighteenth Dynasty, ruling in 1473–1458 BC (Shaw and Nicholson 1995: 311).

Hatshepsut's temple in Deir el-Bahari is an outstanding building in ancient Egyptian architecture, unique in its plan, form and decoration. It is a prominent landmark seen from afar, dominating the valley of Asasif together with the holy mountain of el-Kurn behind it. Its terrace situation and portico design are discernible upon drawing near. A long processional avenue led up to it from the Nile. The vast paved courtyards in front of the lower and middle terraces were surrounded by a high enclosure wall (Pawlicki 2000: 61). The upper portico was decorated with 26 statues of the queen set by the pillars and side walls of the portico. The statues show the queen in the body of Osiris, Lord of the Underworld. A granite gate leading to the upper temple terrace marks the axis of symmetry of the portico. The terrace may be divided into three complexes. The Main Sanctuary of Amun occupies the central part with courtyard and sanctuary. To the south of it there is the Royal Mortuary Cult Complex and to the north, the Sun Cult Complex (Karkowski 2001: 102, 121, 124).

SAMPLING LOCATIONS

Mortar samples were taken in the vestibule of the Altar Courtyard in the Sun Cult Complex and in the vestibule of the Chapel of Hatshepsut in the Royal Mortuary Cult Complex. The whitewash sample comes from the ceiling of the Chapel of Hatshepsut. The following order of samples has been adopted [*Fig. 1*]:

- vestibule of the Sun Cult Complex: base of column on the northern side CSC-K1, center column CSC-K2, column on the southern side CSC-K3, east wall CSC-V1, CSC-V2;
- vestibule of the Chapel of Hatshepsut CRM-V, whitewash from the Chapel of Hatshepsut CRM-CH.

All the samples had the form of fine white powder. Under a stereoscopic microscope most of them were found to contain clumped, worn concentrations of gypsum binder/aggregate and very fine fragments of limestone (ocher color) demonstrating different degrees of weathering. The mortar samples contain small amounts of fine quartz grains, mainly colorless, but also tinted pink, as well as tiny fragments of plant fiber (samples CSC-V2, CRM-V, CSC-V1). The whitewash sample (CRM-CH) is somewhat different in appearance, being made up of fine peeled fragments of bonded lime binder, white in color, featuring contaminating particles seen on the surface, possibly remains of the painting layer.

METHODOLOGY

The research methodology currently in use for historical mortars (Maravelaki-Kalaitzaki et al. 2005: 1578; Iordanidis et al. 2011: 578) marshals a set of advanced

instrumental analyses, which produce a full characteristic of the studied material. It is made possible by the mutually complementary information produced by

the different research methods. The most important ones are: optical microscopy in polarized light (OM), sieve analysis (SA), chemical analysis (ChA), scanning electron microscopy (SEM-EDS), thermal analysis (DTA-TG), X-ray diffraction (XRD), and Fourier transform infrared spectroscopy (FTIR). These analytical methods currently in use are a development of a narrowed methodology adopted in the 1960s, based mostly on chemical analysis at the time (Jędrzejewska 1960). It often led to considerable difficulties in interpreting the results (Elsen 2006: 1417). A growing interest in topics related

to historical mortars resulted in 2000 in several researchers working within the frame of the RILEM International Technical Commission (Middendorf et al. 2000; van Balen et al. 2000; Martinet and Quenee 2000) proposing a set of recommendations and working procedures describing successive steps to be taken in order to obtain detailed information on the binder, filler and mutual binder/filler relation. Arıoğlu and Acun (2006: 1226) proposed a detailed working sequence, taking into consideration the expected outcome of the research in the form of mortars to be

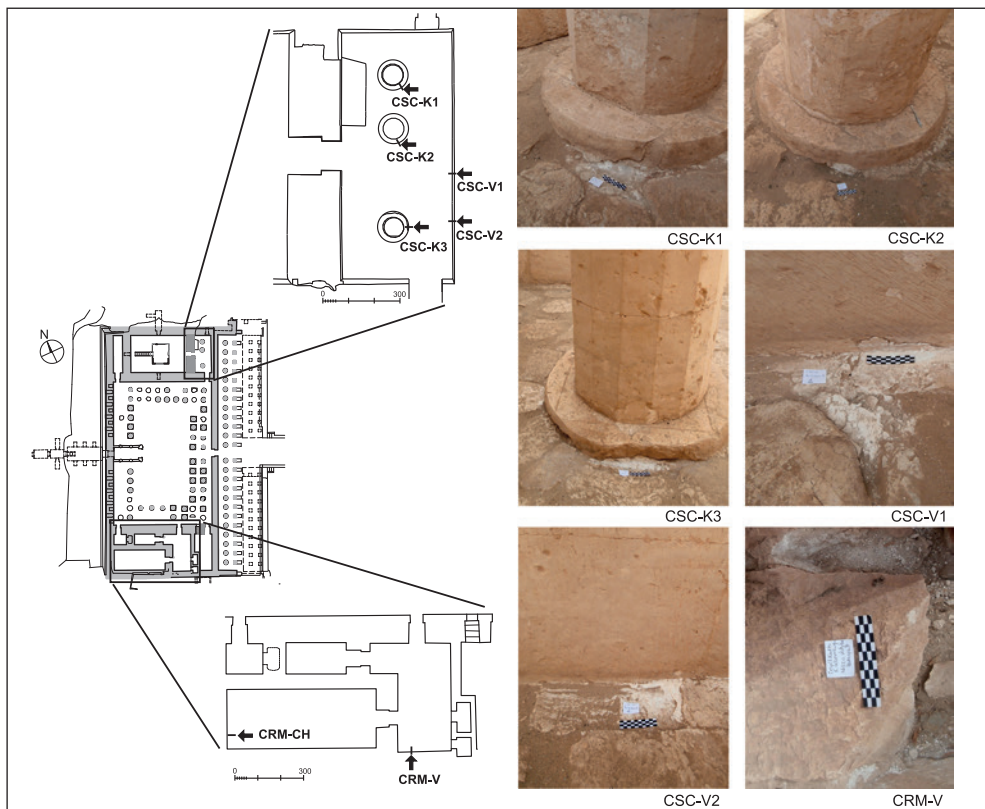


Fig. 1. Sampling locations marked on the plan of the Upper Terrace (Plan and photos T. Dziedzic)

used for restoration filling, complementary with the original historical mortars. Keeping these recommendations in mind, the present authors decided to use only three of the recommended methods: 1) optical microscopy, 2) scanning electron microscopy, and 3) thermal analysis. The decision was determined by the small quantities of historical material for analysis, insufficient for the sieving analysis, for example, where the recommendation for sample weight is at least 100 g (Hauková, Frankeová, and Slížková 2013: 3).

Thin sections for optical microscopy were prepared in the Grinding shop of the Institute of Geological Sciences of the University of Wrocław, following procedures described in available literature (Elsen 2006: 1417–1418; Blaeuer and Kueng 2007: 1201–1202). Samples were impregnated in Canada balsam and cut using a diamond circular saw. They were subsequently attached with epoxy resin exhibiting a refractive index of 1,54 to the microscope slide, polished with polishing powder down to about 30 μm thickness of material (mortar). The thin sections were covered after polishing with a covering glass, glued with Canada balsam. Thin sections were examined under a Zeiss Axiolab polarizing

microscope equipped with a Canon G3 digital camera, which was used for thin-section photography. Modal analysis was done with the point-counting technique described by Roduit (2007: 84–87). For each thin section a set of digital photos were taken and merged together, covering their entire surface. Approximately 900–1000 points were counted in random grid.

Small crumbs of samples were coated with gold for the purposes of scanning electron microscopy. Observations were carried out at the Laboratory for Technological and Conservation Research of the Faculty of Architecture of the Wrocław University of Technology, using the Vega LSU Tescan system with RTG EDS INCA Penta-FETx3 Oxford Instruments with 20 kV acceleration voltage.

The thermal analysis (DTA-TG) was carried out at the Laboratory for Technological and Conservation Research of the Faculty of Architecture of the Wrocław University of Technology, using a Netzsch STA 409 thermal analyzer. Analysis conditions: (1) sample mass varying between 18 mg and 30 mg, (2) ceramic Al_2O_3 pans with pin-holed lids, (3) temperature range 40–1000°C, (4) heating rate 10°C/min., (5) atmosphere N_2 .

OPTICAL MICROSCOPY (OM)

Petrographic studies have shown that the mortar samples studied for the project differ in terms of the nature of the binder, while the filler represents a similar, highly dispersed granular framework. The binder is microcrystalline and polymineral in nature [Fig. 2], a mass that is not homogeneous, consisting of gypsum microflakes and grains of calcium carbonate in micrite

form. In most of the samples (CSC-K1, CSC-K2, CSC-K3, CRM-V, CSC-V1; see Fig. 2) the microcrystalline binder is tinted a weak brown that is definitely lighter in tone than the typical micrite. In cross-polarized light the binding mass reveals birefringence colors, both of the first order, gray, typical for gypsum and of the high order, indicating the presence

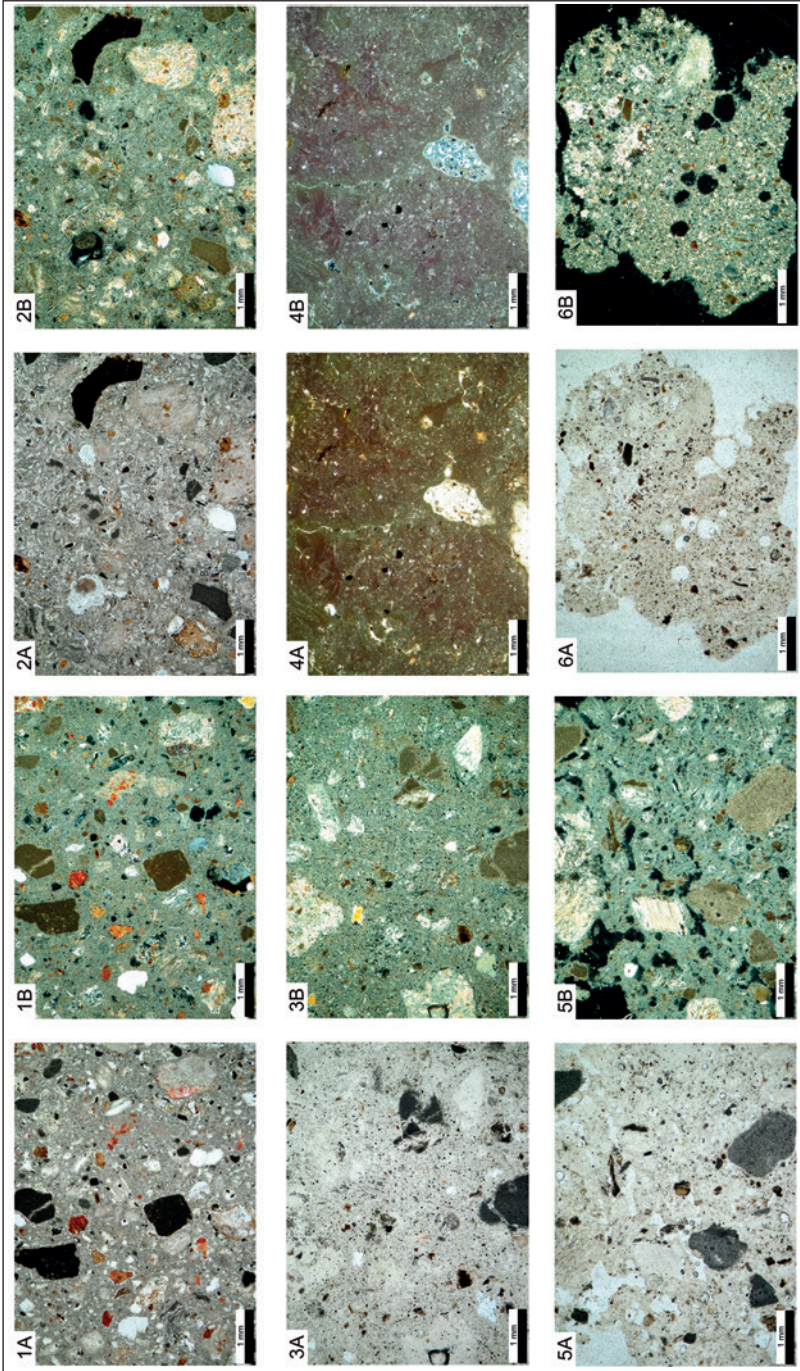


Fig. 2. Microphotographs of mortar samples: 1 – CSC-K1, 2 – CSC-K2, 3 – CSC-K3, 4 – CSC-V2, 5 – CRM-I, 6 – CSC-V1, taken in plane-polarized light (A) and cross-polarized light (B)

of a strong birefringent crystalline phase like calcium carbonate. Both single crystals and polycrystalline grains of anhydrite can be observed in most of the samples. In mortars represented by samples CSC-K2 and CRM-V this phase is present usually as single crystals, under 0.1 mm in size. Polycrystalline aggregates of anhydrite reaching 1.0 mm in size as well as numerous single crystals occur in the mortar of sample CSC-V1 [Fig. 2].

The binder of sample CSC-V2 is different in nature [Fig. 2]. The microcrystalline mass is heavily browned in plane-polarized light and shows a strong birefringence under crossed polarizers; it is composed of micrite. Sporadically in the micrite there occur small zones of irregular shape, 1.0–1.5 mm in size, composed of polymineral binder, similar to that of sample CSC-V1. They are formed of a microcrystalline mass of gypsum crystals and calcium carbonate, and small but relatively numerous crystals of anhydrite.

The filler in all the samples is relatively not abundant. It consists mainly of irregularly shaped, angular grains up to approximately 1.0 mm in size [Fig. 2]. Part is colorless, composed of gypsum crystals of a size much larger than the same component in the binder. These represent gypsum rock fragments. Others are brown or orange-brown in color and represent carbonate rocks or transitional type rock: micritic limestone or marls. They are particularly abundant in samples CSC-K1, CSC-K2, CSC-K3, CRM-V, less abundant and smaller in size in the mortar of sample CSC-V1. Some of the limestone grains are composed of a micritic mass representing micritic limestone (micrite, Folk 1959), or micrite and sparite (dismicrite, Folk 1959). Grains

of biogenic limestone (biomicrite, Folk 1959) are very rare; they are composed of a micritic matrix and numerous bioclasts (foraminifera). Apart from limestone and gypsum rocks, quartz grains and very seldom feldspars and fragments of magmatic rocks occur. The latter are present solely in samples CSC-K1 and CSC-K2. Quartz, feldspar and magmatic rocks occur in the form of small weakly rounded grains not exceeding about 0.3 mm in size. Auxiliary components supplement the matrix-supported framework, but often it is no more than a few grains per thin-section. These are: epidote (samples CSC-K1, CSC-K2), amphibole (samples CSC-K1, CSC-K3), glauconite (sample CSC-K2), organic substance (samples CSC-K1, CRM-V, CSC-V1), and opaques (samples CSC-V2, CSC-V1).

THERMAL ANALYSIS (DTA-TG)

Thermal analysis of all the samples demonstrated a relatively small weight loss in temperatures up to 105°C, usually not exceeding 0.20% of the total weight [Table 1, Fig. 3]. Larger weight loss (0.43%) was shown only by sample CSC-K1 [Table 1, Fig. 3:A]. This weight loss is accompanied by a very small endothermic effect, registered by the DTA curve, and interpreted as a process of loss of hygroscopic water (Maravelaki-Kalaitzaki et al. 2005: 1579; Iordanidis et al. 2011: 580). In the temperature range of 105–200°C weight loss is much greater, ranging between 0.18% to 0.88% of the weight [Table 1, Fig. 3]. For samples with relatively little weight loss in the given temperature range (e.g., CSC-K1), the DTA curve shows weak endothermic effect. DTA-TG diagrams of samples demonstrating

higher weight loss in the 105–200°C range record a strong deflection of the TG curve associated with a strong endothermic peak marked on the DTA curve (e.g., sample CSC-K3, *Fig. 3:C*). Changes of mass are recorded on the TG curve for a narrow temperature range of 125–135°C [*Fig. 3*]. The thermal effects in the 105–200°C range, in which the said reactions occur, are interpreted usually in the case of historical mortars as a gypsum dehydration effect. For natural rock the process takes place in two stages expressed as a characteristic doublet on TG as well as DTA curve (Wyrwicki 1988: 46). In the first stage of dehydration, gypsum releases 1.5 molecules of water and a hemihydrate is formed. In the second stage, in temperatures below 200°C, the hemihydrate loses the rest of the water (0.5 molecule of H₂O) and forms an anhydrous form anhydrite γ -CaSO₄ (Wyrwicki 1988: 46; Ramachandran et al. 2002: 450). The absence of a doublet typical of gypsum dehydration in the TG and DTA curves, as well as the considerably lower temperature for gypsum

dissociation most probably is due to the low content of this component in the sample (Ramachandran et al. 2002: 459). Strong pulverization of the sampled substance surely results in a lowered temperature, as does also the use of a sealed crucible and the occurrence in the sample of thermally inactive substances (Stoch 1974: 120–128). Dehydration of clay minerals takes place in a similar temperature range (the maximum for illite is about 130°C; Wyrwicki 1988: 30), but in most of the DTA-TG diagrams the process of their dehydroxylation (endothermic and weight loss effect), which typically reaches a maximum for illite at about 540°C is not well marked (Wyrwicki 1988: 30). However, the presence of clay minerals appears to be confirmed by the diagram obtained for manually separated material from sample CRM-V [*Fig. 3:F*]. Most of the analyzed samples demonstrated a quasi-constant weight loss in the 200–600°C range. The sole exceptions are samples CSC-V1 [*Fig. 3:G*], and especially CRM-CH [*Fig. 3:H*] which show a weak inflection

Table 1. Weight loss of samples subjected to thermal analysis (DTA-TG) in weight % (temperature ranges after: Moropoulou, Bakolas, and Bisbikou 1995; Biscontin, Pellizon Birelli, and Zendri 2002; Maravelaki-Kalaitzaki et al. 2005; Bultrini et al. 2006)

Sample	Weight loss [% weight] in specific temperature range [°C]			
	< 105°C	105–200°C	200–600°C	> 600°C
CSC-K1	0.43	0.18	1.28	12.21
CSC-K2	0.09	0.49	1.33	7.85
CSC-K3	0.02	0.77	1.29	9.47
CSC-V2	0.19	0.59	2.20	11.07
CRM-V	0.12	0.44	2.03	6.52
CRM-Vg*	0.95	1.09	4.37	16.49
CSC-V1	0.12	0.37	1.95	9.81
CRM-CH	0.05	0.88	3.22	34.54

* Sample CRM-V subjected to manual grain separation using a stereomicroscope.

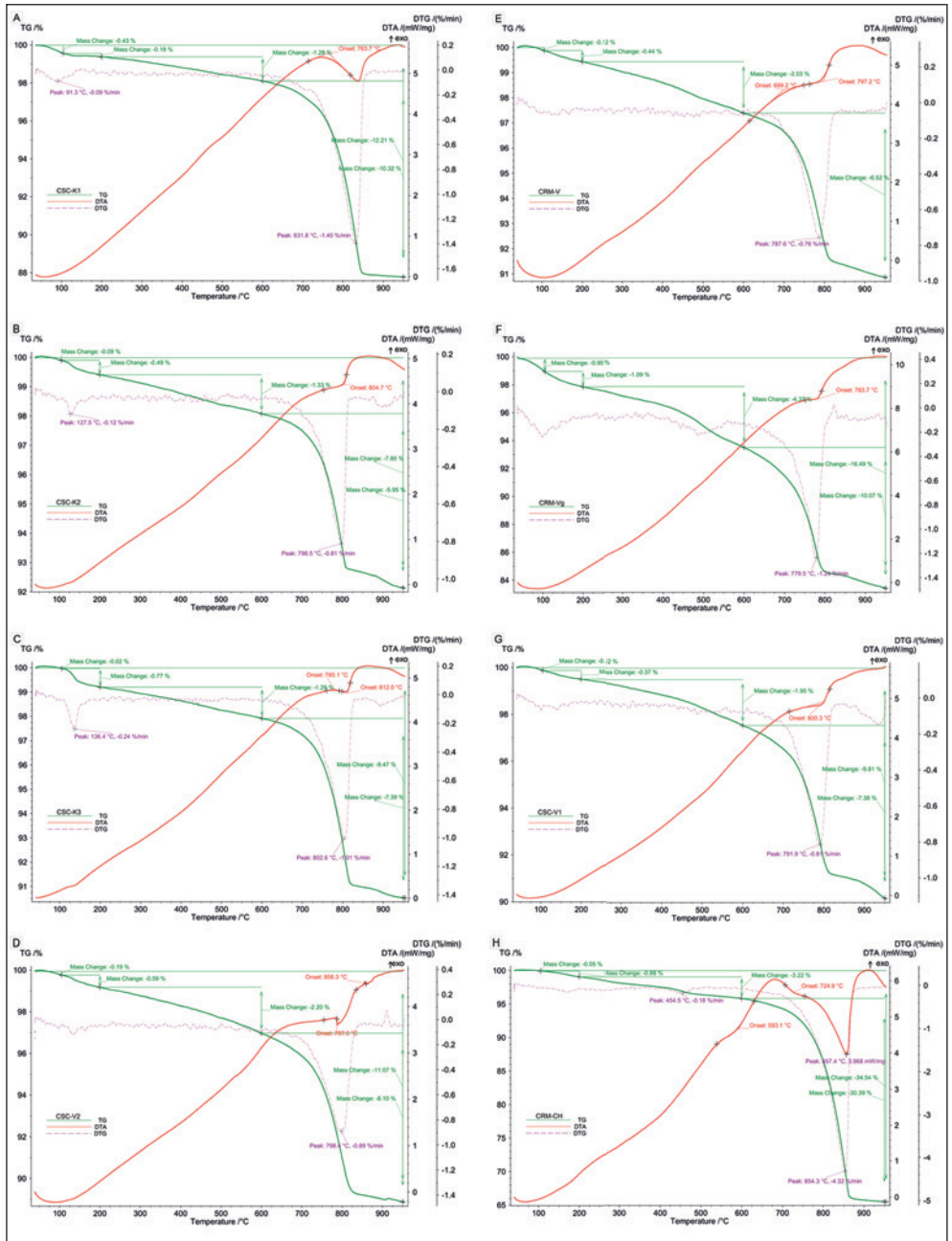


Fig. 3. DTA-TG curves for mortar samples: A – CSC-K1, B – CSC-K2, C – CSC-K3, D – CSC-V2, E – CRM-V, F – CSC-V1, G – CRM-CH

of the TG curve at temperatures of about 500°C (CSC-V1) and 454°C (CRM-CH) respectively. Owing to the fact that both samples show weight loss in the 105–200°C range, which is to be interpreted as among others clay minerals dehydration effect, this effect could also be related to their dehydroxylation. It occurs at 350–700°C for illite with a peak at about 540°C (Wyrwicki 1988: 30). Dehydroxylation of portlandite (calcium hydroxide; Moropoulou, Bakolas, and Bisbikou 1995: 785) occurs at about 450°C, but in view of the age of the samples the presence of unreacted slaked lime seems improbable. These effects may be due to the thermal dissociation of magnesite, a component of some mortars, which decomposes in a temperature of 480°C (Bruni et al. 1998: 163; Montoya et al. 2003: 113–114), although it is relatively seldom encountered. It is more likely that the quasi-constant weight loss in the 200–600°C range is caused by the dissociation of iron oxyhydroxide (III), the main component of goethite, a ferrous mineral common in nature, the dissociation process of which takes place in the 200–700°C temperature range with peaks at about 300–400°C (Wyrwicki 1988: 38). In summary, the absence of an evident and strong endothermic effect makes it practically impossible to associate the weight-loss effect with a given stage.

In the case of samples CRM-CH, another endothermic effect is recorded as a slight inflection on the DTA curve at 570°C [Fig. 3:H] coupled with no weight loss. This may be related to the effect of a polymorphic transformation of low-temperature quartz into its high-temperature modification, occurring at

573°C (Deer, Howie, and Zussman 1992: 464).

All the mortar samples record the greatest weight loss at temperatures above 600°C, from 6.52% to 34.54% [Table 1, Fig. 3]. A well pronounced inflection of the TG curve is associated with a strong endothermic effect. Thermal reactions above this temperature are interpreted usually as the effect of carbonate (calcite, dolomite) dissociation producing gaseous CO₂ (Wyrwicki 1988: 40–42; Biscontin, Pellizon Birelli, and Zendri 2002: 35). Natural calcite decomposes in temperatures much higher than 600°C (Wyrwicki 1988: 40). In the case of mortar, however, there is a similar trend observed as for gypsum, that is, a lowered temperature for starting a reaction. Moreover, the broad temperature range for carbonate dissociation, starting at 600°C, is believed to be caused by the presence of a microcrystalline form due to slaked-lime carbonation (Marques et al. 2006: 1899). Furthermore, the presence of two endotherms is related to the additional presence of well crystallized calcite, which is usually a component of carbonate fillers (Marques et al. 2006: 1899). For some samples (CSC-K1, CSC-V2, CRM-CH) the TG curve rapidly flattens, which is typical behavior for the end of calcite thermal dissociation [Fig. 3:A,D,H]. The presence of two different forms of crystalline calcium carbonate may explain the fairly atypical shape of the TG curve for the remaining samples, where substantial progressing weight loss occurred after the flattening at about 800°C. A two-stage weight loss is evident in the case of sample CSC-V1 [Fig. 3:G], for example. The DTA curve demonstrates two inflections: at 791°C and at about

960°C. Dolomite undergoes a two-stage dissociation in a similar temperature range, but the two thermal effects should be strongly marked on both the TG and DTA curves. No such evident mark has been observed on the diagrams for the second effect. It cannot be excluded that the inflection in the TG curve above the temperature for carbonate dissociation points to the presence of muscovite or sericite, which is a microcrystalline form of muscovite. The dehydroxylation of this mineral takes place at 700–950°C with a peak at 850°C (Schomburg 1991: 216), although according to some authors, the phase may remain stable until 950°C is crossed (Palanivel and Rajesh Kumar 2011: 202).

SCANNING ELECTRON MICROSCOPY (SEM)

Scanning electron microscopy of the samples demonstrated the microcrystalline nature of the binder which is considerably porous [Fig. 4:1–6]. Fine microcrystals in the binder tend to form small isometric aggregates of varying size, reaching a maximum of 50µm [Fig. 4:3, 5]. Joining surfaces are small as a rule, creating a characteristic foamy structure. Differentiated aggregate size results in a broad range of pore size and consequently volume, the diameter reaching 20–30 µm [see Fig. 4:3, 5 and 4]. The binder is predominantly composed of very fine anhedral crystals making up the said massive aggregates [Fig. 4:3]. Subhedral crystals of platy or needle-shaped form were observed growing on these aggregates [Fig. 4:2, 4, 5], less frequently forming euhedral crystals similar to a rhomboedron [Fig. 4:2]. The size of such crystals did not exceed about 10µm.

SEM-EDS measurements showed that for the most of the analytical points the elemental composition was restricted to oxygen, sulphur and calcium [Fig. 4:1 spectra A, B, C; 4:2 spectrum C; 4:3 spectra B, D; 4:4 spectra C, D; 4:5 spectra A, D; 4:6 spectrum B)]. Very seldom the obtained spectra show peaks related to silicon, sporadically carbon [Fig. 4:1 spectrum D; 4:2 spectrum D, 4:4 spectrum A; 4:5 spectrum B, 4:6 spectra A, C]. The elemental composition indicates that the binder is composed of calcium sulfates (gypsum $\text{CaSO}_4 \cdot 2\text{H}_2\text{O}$, anhydrite CaSO_4), contaminated by a small amount of silica found presumably in the structure of small grains of quartz or cryptocrystalline chalcedony (SiO_2). Rare presence of carbon indicates that calcium carbonates (calcite CaCO_3) play a subordinate role in binding the matrix. EDS showed strong peaks of calcium and much weaker ones of oxygen, carbon and occasionally sulphur [Fig. 4:2 spectra A, B]. Characteristic subhedral, rhombohedral shaped crystals occurred here. Their morphology and chemical composition suggest they are calcium carbonate (calcite). Small intensity peaks of sulphur and silica were identified occasionally next to those described above [Fig. 4:3 spectrum A]. The binder in such places was composed most likely of intergrowth of calcium sulphates and carbonates. The silica originated most probably from cryptocrystalline silica (quartz, chalcedony) dispersed in the binder. Sporadically the EDS spectrum shows the presence of calcium, oxygen, carbon, sulphur, silica and magnesium [Fig. 4:3 spectrum C; 4:4 spectrum B, 4:5 spectrum C]. It probably reflects intergrowth of microcrystals of calcium

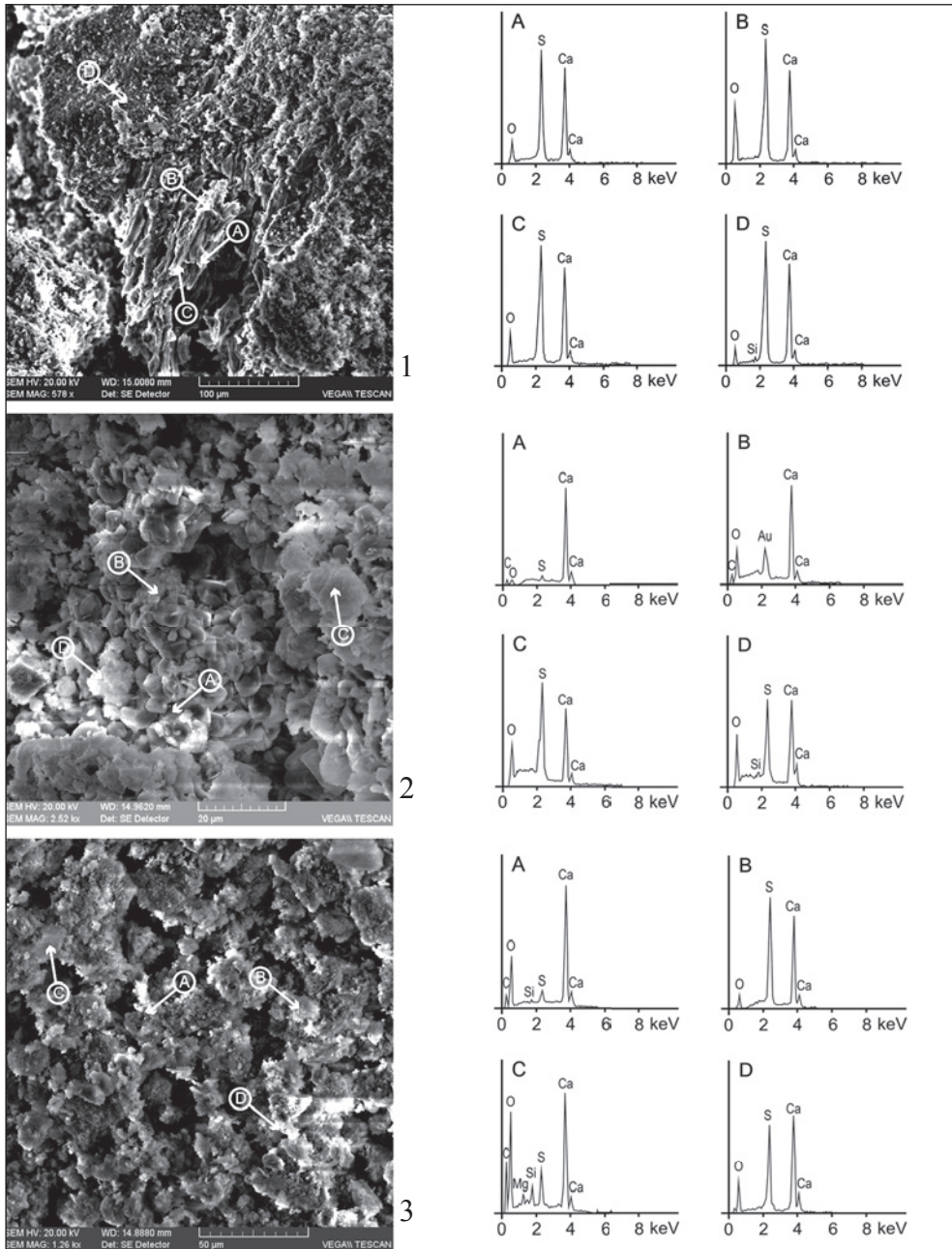


Fig. 4. SEM-SE images of mortar samples and representative EDS spectra for the samples: 1 – CSC-K1, 2 – CSC-K2, 3 – CSC-K3 (for samples 4, 5, 6, 7 see the following pages)

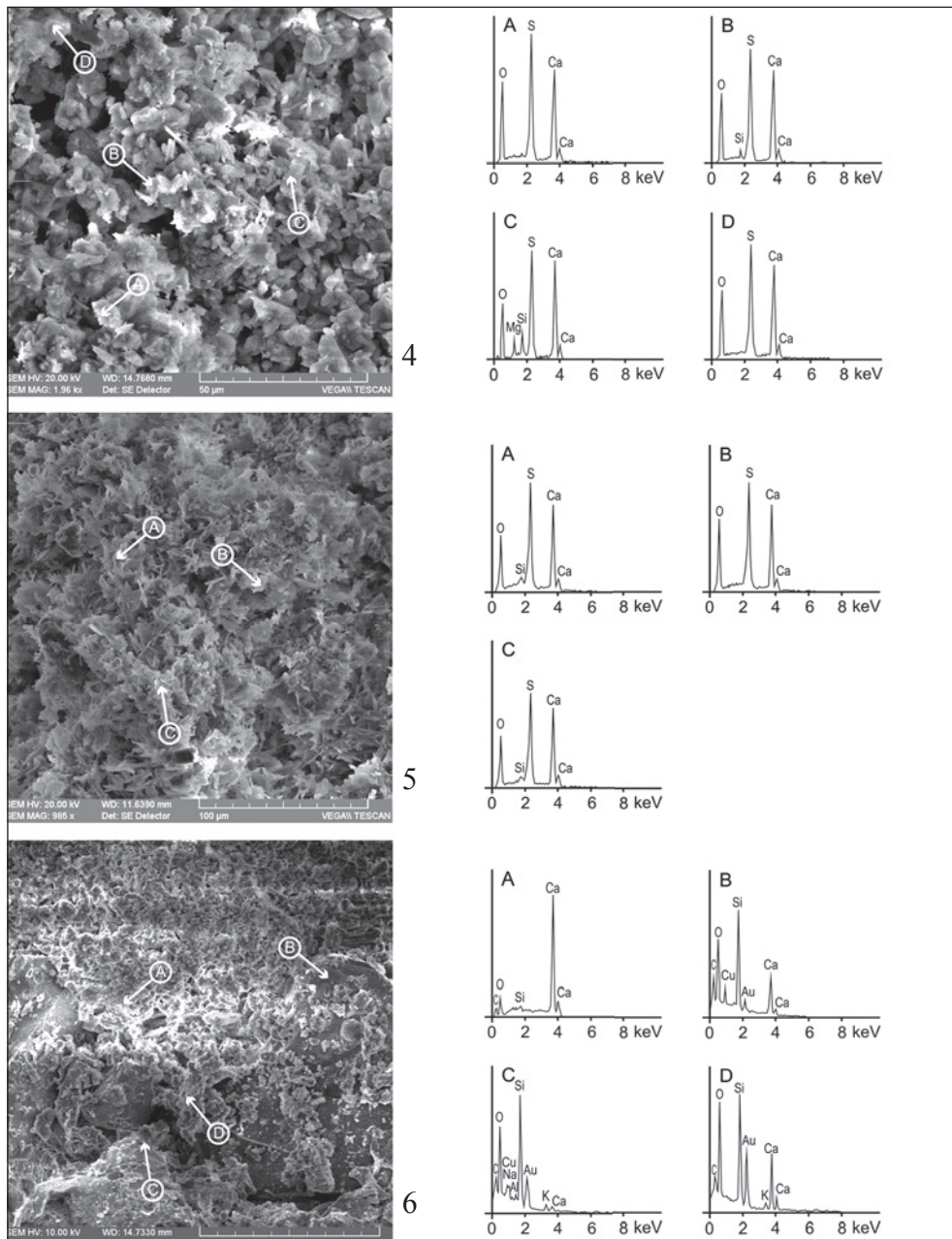


Fig. 4 continued. SEM-SE images of mortar samples and representative EDS spectra for the samples: 4 – CSC-V2, 5 – CRM-V, 6 – CSC-V1 (for samples 1, 2, 3, and 7, see the preceding and following pages)

sulphates (gypsum, anhydrite), calcium and magnesium carbonates (calcite and magnesite or dolomite $\text{CaMg}[\text{CO}_3]_2$), containing dispersed microcrystalline silica or fine quartz.

Samples of whitewash CRM-CH gave a different picture. The binder is a microcrystalline mass, relatively compact, composed of slightly elongated crystals [Fig. 4:7], dominated by calcium, oxygen, carbon and some silica [Fig. 4:7 spectra A, D]. The shape and composition point to crystals of calcium carbonate (calcite). Silicon comes presumably from the silica dispersed in the binder. The grains of the filler are several dozen micrometers in diameter. The binding mass adhere to them well, rarely leaving small voids [Fig. 4:7]. The composition of grains is strongly differentiated, with a predominance of silicon and oxygen [Fig. 4:7 spectrum B], suggesting a grain of quartz in this case. The calcium and carbon result from carbonate binder enveloping the grain. The presence of copper is presumably

due to a paint layer on the surface slowly migrating over time into the interior of the mortar. The copper could also reflect the use of tools made of a copper alloy used for natural stone mining, the stone then being used as filler. Grains of feldspar have also been noted [Fig. 4:7 spectrum C]. Beside oxygen, silica and aluminum they also contain potassium and sodium, both of which can be seen in the spectrum. The calcium, carbon and part of the oxygen registered in the spectrum probably come from the binder particles preserved on the surface of the analyzed grain [Fig. 4:7 spectrum C].

X-RAY DIFFRACTION (XRD)

X-ray diffraction analyses proved that anhydrite and calcite are the main crystalline phases found in the investigated mortars. They give the most intense peaks on the diffraction patterns [Fig. 5]. Quartz is a subordinate component. Its highest peak ($2\theta = 31.04^\circ$) has a variable intensity on the diffraction patterns. It was strong for

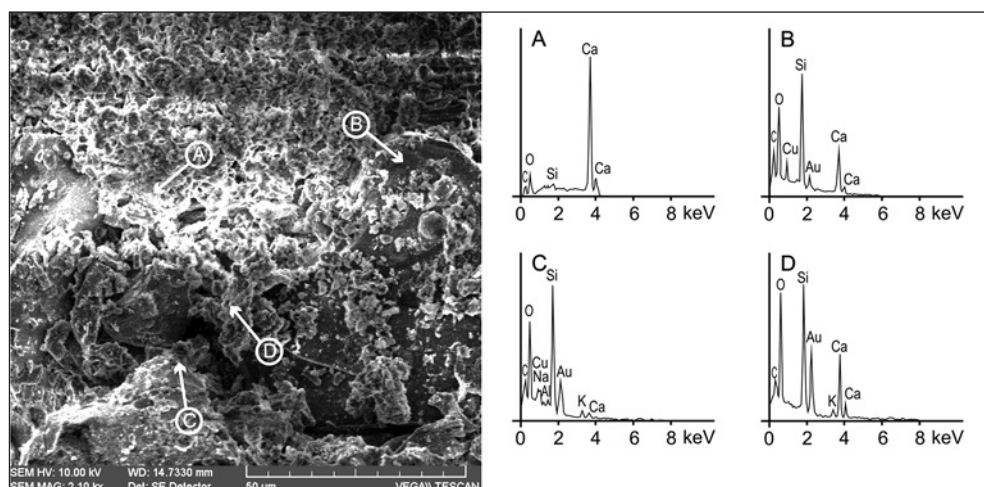


Fig. 4 continued. SEM-SE images of mortar samples and representative EDS spectra for the sample: 7 – CRM-CH (for samples 1–6 see the preceding pages)

mortar samples CRM-V and CSC-V2, but much less intense for samples CSC-K3, CSC-K2, CSC-K1 and CSC-V1. This relative differentiation of quartz peak intensities indicates its variable content. It is more abundant in the first two samples compared to the last-mentioned samples. Gypsum is another mineral present in all of the samples, manifested in the diffraction patterns by relatively weak peak intensities. The most intense peak for this mineral phase, $2\theta=36.31$, is best observed in the diffraction pattern for samples CSC-V2 and CRM-V; in the case of the remaining samples, it is very weakly marked. Inferred quantities of gypsum are confirmed also by the absence of the next intense peak for this mineral phase, which should appear in the diffraction patterns for $2\theta=24.13$. There is only a raised background for this 2θ value with a weak peak marked only for

sample CSC-K3. Feldspar minerals were also identified (both Ca–Na feldspars and alkali feldspars); weak peaks were observed for $2\theta=32.36$ (diffraction pattern for sample CSC-V1 in *Fig. 3:F*) and $2\theta=32.04$ (diffraction pattern for sample CRM-V). Poorly marked peak for $2\theta=49.77$ is probably sylvine (KCl). The diffraction pattern of this mineral shows another intense peak at $2\theta=34.3$, but is overlapped with the calcite peak. Hence the presence of sylvine in these samples is not confirmed for certain. It cannot be excluded that this peak derives from siderite (FeCO_3). The presence of dolomite, at least in some of the samples, is also possible, as suggested by the broader peak at $2\theta=36.12$. Its shape is due to the occurrence of dolomite and gypsum peaks directly next to each other, which is best observed for samples CSC-V2 and CRM-V [see *Fig. 5*].

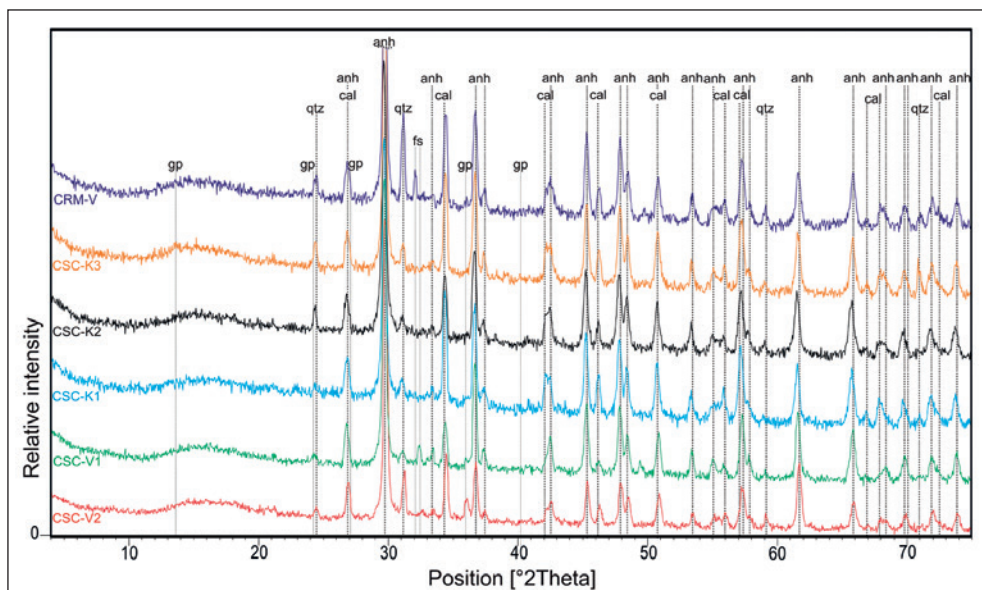


Fig. 5. X-ray diffraction patterns

SUMMARY

The analyses of mortar samples from the Temple of Hatshepsut in Deir el-Bahari have demonstrated that the main components of the binder were calcite, gypsum and anhydrite, whereas the filler was composed of quartz, feldspar and fragments of sedimentary rocks with subordinate magmatic rocks. Most of these components constitute alluvial deposits (river deposits), present in the Nile Valley. The limestone and anhydrite came from the rocks forming the cliff that rises behind the temple, composed of the Esna Shale Formation (argillaceous schist, marls) overlain by the Thebes Limestone Formation (limestone rich in foraminiferas) (Dupuis et al. 2011: 247–250). Both formations contain anhydrite, which often forms anhydrite nodules (Wüst and Schlüchter 2000: 1162, 1165).

The binder of the mortars sampled from different parts of the temple, polymineral and microcrystalline in form, differs from sample to sample. It is a heterogenous mass, heavily porous and composed of gypsum and calcite (micrite) in differing proportions. Sample CSC-V2 differs substantially from the others by the relatively abundant presence of

small crystals of anhydrite. It leads to the conclusion that a different mortar was used in this part of the Vestibule of the Sun Cult Complex. The results of the study will contribute to a better understanding of the chronology of the various building and rebuilding stages that are suggested for the Sun Cult Complex.

Whitewash sample (CRM-CH) is free from the filler and composed of the binder, formed as a microcrystalline and dense mass consisting of micrite grains. It should be emphasized that it would be valuable to continue the research, but extended on a broader scale and representative for the whole building material (samples taken at different locations in the temple). Analysis of additional samples would allow better understanding of mortar composition, used for construction of one of the most important buildings in the history of architecture. The results reported in this study are too limited in terms of the analytic material to be useful in chronological stratification of the temple, especially as the mortars that were sampled for this analysis proved to be relatively homogeneous.

Dr. Teresa Dziedzic

Wrocław University of Technology, Faculty of Architecture
50-317 Wrocław, Poland, ul. Bolesława Prusa 53/55
teresa.dziedzic@pwr.edu.pl

Wojciech Bartz

University of Wrocław, Faculty of Earth Sciences and Environmental Management,
Institute of Geological Sciences
50-205 Wrocław, Poland, ul. Cybulskiego 30
wojciech.bartz@ing.uni.wroc.pl

Maria Gašior

Wrocław University of Technology, Faculty of Architecture, Laboratory for Technological and Conservation Research

50-334 Wrocław, Poland, ul. Rozbrat 7

ltk@pwr.edu.pl

REFERENCES

- Arioglu, N., & Acun, S. (2006). A research about a method for restoration of traditional lime mortars and plasters: A staging system approach. *Building and Environment*, 41(9), 1223–1230.
- Arnold, D. (1991). *Building in Egypt: Pharaonic stone masonry*. Oxford: Oxford University Press.
- Arnold, D., Gardiner, S. H., Strudwick, H., & Strudwick, N. (2003). *The encyclopedia of ancient Egyptian architecture*. Princeton, NJ: Princeton University Press.
- Biscontin, G., Pellizon Birelli, M., & Zendri, E. (2002). Characterization of binders employed in the manufacture of Venetian historical mortars. *Journal of Cultural Heritage*, 3(1), 31–37.
- Blaeuer, C., & Kueng, A. (2007). Examples of microscopic analysis of historic mortars by means of polarising light microscopy of dispersions and thin sections. *Materials Characterization*, 58(11–12), 1199–1207.
- Bruni, S., Cariati, F., Fermo, P., Pozzi, A., & Toniolo, L. (1998). Characterization of ancient magnesian mortars coming from northern Italy. *Thermochimica Acta*, 321(1–2), 161–165.
- Bultrini, G., Fragala, I., Ingo, G. M., & Lanza, G. (2006). Mineropetrographic, thermal and microchemical investigation of historical mortars used in Catania (Sicily) during the XVII century A.D. *Applied Physics A*, 83(4), 529–536.
- Clarke, S., & Engelbach, R. (1990). *Ancient Egyptian construction and architecture*. New York: Dover Publications.
- Deer, W. A., Howie, R. A., & Zussman, J. (1992). *An introduction to the rock-forming minerals* (2nd ed.). Harlow: Longman Scientific & Technical.
- Dupuis, C., Aubry, M.-P., King, C., Knox, R. W. O., Berggren, W. A., Youssef, M., Fathi Galal, W., Roche, M. (2011). Genesis and geometry of tilted blocks in the Theban Hills, near Luxor (Upper Egypt). *Journal of African Earth Sciences*, 61(3), 245–267.
- Elsen, J. (2006). Microscopy of historic mortars – A review. *Cement and Concrete Research*, 36(8), 1416–1424.
- Folk, R. L. (1959). Practical petrographic classification of limestones. *American Association of Petroleum Geologists Bulletin*, 43(1), 1–38.
- Hauková, P., Frankeová, D., & Slížková, Z. (2013). Characterisation of historic mortars for conservation diagnosis. In J. J. Hughes (Ed.), *3rd Historic Mortars Conference: HMC 13, Glasgow, 11–13 September 2013*. Glasgow: University of the West of Scotland.
- Iordanidis, A., Garcia-Guinea, J., Strati, A., Gkimourtzina, A., & Papoulidou, A. (2011). Thermal, mineralogical and spectroscopic study of plasters from three post-Byzantine churches from Kastoria (northern Greece). *Journal of Thermal Analysis and Calorimetry*, 103(2), 577–586.
- Jędrzejewska, H. (1960). Old mortars in Poland: A new method of investigation. *Studies in Conservation*, 5(4), 132–138.

- Karkowski, J. (2001). The decoration of the Temple of Hatshepsut at Deir el-Bahari. In Z.E. Szafranski (Ed.), *Królowa Hatszepsut i jej świątynia 3500 lat później = Queen Hatshepsut and her temple 3500 years later* (pp. 99–157). Warsaw: Agencja Reklamowo-Wydawnicza A. Grzegorzcyk.
- Lipińska, J., & Koziński, W. (1977). *Cywilizacja miedzi i kamienia: technika starożytnego Egiptu [Civilisation of copper and stone: The technology of Ancient Egypt]*. Warsaw: Państwowe Wydawnictwo Naukowe [in Polish].
- Lucas, A. (1948). *Ancient Egyptian materials and industries* (3rd ed., rev.). London: Arnold.
- Lucas, A., & Harris, J. R. (1962). *Ancient Egyptian materials and industries* (4th ed., rev.). London: Arnold.
- Maravelaki-Kalaitzaki, P., Bakolas, A., Karatasios, I., & Kilikoglou, V. (2005). Hydraulic lime mortars for the restoration of historic masonry in Crete. *Cement and Concrete Research*, 35(8), 1577–1586.
- Marques, S. F., Ribeiro, R. A., Silva, L. M., Ferreira, V. M., & Labrincha, J. A. (2006). Study of rehabilitation mortars: Construction of a knowledge correlation matrix. *Cement and Concrete Research*, 36(10), 1894–1902.
- Martinet, G., & Quenee, B. (2000). Proposal for a useful methodology for the study of ancient mortars. In P. Bartos, C. Groot, & J. J. Hughes (Eds.), *International RILEM Workshop on Historic Mortars: Characteristics and Tests, Paisley, Scotland, 12th–14th May 1999* (pp. 81–91). Cachan: RILEM Publications.
- Middendorf, B., Baronio, G., Callebaut, K., & Hughes, J. (2000). Chemical-mineralogical and physical-mechanical investigations of old mortars. In P. Bartos, C. Groot, & J. J. Hughes (Eds.), *International RILEM Workshop on Historic Mortars: Characteristics and Tests, Paisley, Scotland, 12th–14th May 1999* (pp. 53–59). Cachan: RILEM Publications.
- Montoya, C., Lanás, J., Arandigoyen, M., Navarro, I., García Casado, P. J., & Alvarez, J. I. (2003). Study of ancient dolomitic mortars of the church of Santa Maria de Zamarce in Navarra (Spain): Comparison with simulated standards. *Thermochimica Acta*, 398(1–2), 107–122.
- Moropoulou, A., Bakolas, A., & Bisbikou, K. (1995). Characterization of ancient, Byzantine and later historic mortars by thermal and X-ray diffraction techniques. *Thermochimica Acta*, 269–270, 779–795.
- Nicholson, P. T., & Shaw, I. (2000). *Ancient Egyptian materials and technology*. Cambridge: Cambridge University Press.
- Palanivel, R., & Rajesh Kumar, U. (2011). Thermal and spectroscopic analysis of ancient potteries. *Romanian Journal of Physics*, 56(1–2), 195–208.
- Pawlicki, F. (2000). *Skarby architektury starożytnego Egiptu: królewskie świątynie w Deir el-Bahari [Architectural treasures of ancient Egypt: The royal temples at Deir el-Bahari]*. Warsaw: Arkady [in Polish].
- Ramachandran, V. S., Paroli, R. M., Beaudoin, J. J., & Delgado, A. H. (2002). *Handbook of thermal analysis of construction materials*. Norwich, NY: Noyes Publications.
- Roduit, N. (2007). *JMicroVision: un logiciel d'analyse d'images pétrographiques polyvalent*. University of Geneva. Retrieved from <http://www.jmicrovision.com/examples/these.pdf> [accessed: 3 February 2014].

- Schomburg, J. (1991). Thermal reactions of clay minerals: Their significance as “archaeological thermometers” in ancient potteries. *Applied Clay Science*, 6(3), 215–220.
- Shaw, I., & Nicholson, P.T. (1995). *British Museum dictionary of ancient Egypt*. London: British Museum Press.
- Stoch, L. (1974). *Minerały ilaste [Clay minerals]*. Warsaw: Wydawnictwa Geologiczne [in Polish].
- van Balen, K., Toumbakari, E.-E., Blanco, M.-T., Aguilera, J., Puertas, F., Sabbioni, C., Zappia, G., Riontino, C., Gobbi, G. (2000). Procedure for a mortar type identification: A proposal. In P. Bartos, C. Groot, & J. J. Hughes (Eds.), *International RILEM Workshop on Historic Mortars: Characteristics and Tests, Paisley, Scotland, 12th–14th May 1999* (pp. 61–70). Cachan: RILEM Publications.
- Wüst, R. A. J., & Schlüchter, C. (2000). The origin of soluble salts in rocks of the Thebes Mountains, Egypt: The damage potential to Ancient Egyptian wall art. *Journal of Archaeological Science*, 27(12), 1161–1172.
- Wyrwicki, R. (1988). *Analiza derywatograficzna skał ilastych [Derivatographic analysis of clay minerals]*. Warsaw: Wydawnictwo Uniwersytetu Warszawskiego [in Polish].